Journal of Power Sources 195 (2010) 787–793

Contents lists available at ScienceDirect

Journal of Power Sources

journal homepage: www.elsevier.com/locate/jpowsour

The effects of wetproofing on the capillary properties of proton exchange membrane fuel cell gas diffusion layers

Joseph D. Fairweather, Perry Cheung, Daniel T. Schwartz*

Electrochemical Materials and Interfaces Laboratory, Department of Chemical Engineering, Box 351750, University of Washington, Seattle, WA 98195-1750, United States

ARTICLE INFO

Article history:
Received 6 July 2009
Received in revised form 12 August 2009
Accepted 13 August 2009
Available online 20 August 2009

Keywords:
Gas diffusion layer
Capillary pressure
Teflon
Contact angle
Water management
Fuel cell

ABSTRACT

In the analysis of proton exchange membrane (PEM) fuel cell components, the capillary pressure vs. saturation ($P_C(S_L)$) curve is an increasingly popular tool for understanding the interaction of liquid water with the porous gas diffusion layer (GDL) material. In this study, hysteretic water/air $P_C(S_L)$ measurements were combined with mercury intrusion porosimetry (MIP) and time-of-flight secondary ion mass spectrometry (ToF-SIMS) imaging to quantify the effects of fluoropolymer loading on GDL samples. Commercially wetproofed carbon fiber papers with 0–40 wt.% Teflon loading were investigated. MIP showed a slight reduction in characteristic pore radii and a significant loss of pore volume at the highest Teflon loading. Water/air $P_C(S_L)$ measurements showed a significant reduction in water wetting between samples with 0 and 5 wt.% Teflon loading, but negligible additional wetproofing at loadings from 10 to 40 wt.%. ToF-SIMS imaging, a technique that is sensitive to monolayer surfaces coverages, found that GDL materials with 5 wt.% Teflon loading displayed nearly complete fluoropolymer coverage on the carbon substrate, confirming $P_C(S_L)$ measurements showing that all of the wetproofing occurs in a narrow range of Teflon loadings. Results for $P_C(S_L)$ measurements were fitted using a bundle-of-capillaries model. The apparent water intrusion contact angles fell between 130° and 133° in the rough Teflonated pore space (regardless of loading), whereas the apparent gas intrusion contact angles fell between 66° and 70° for the same materials.

1. Introduction

Water management continues to be a major research focus for proton exchange membrane (PEM) fuel cells. Poor water management in a PEM system results in either membrane dehydration (decreased ionic conductivity [1]) or flooding and the myriad issues that accompany excess liquid water (including mass transport resistance [1] and faster degradation of stack components [2,3]). The engineering of gas diffusion layers (GDLs) that sustain membrane hydration without flooding over a wide range of operating conditions is one route to better water management. Although the GDL has received much attention for this reason [1,4–10], a fundamental understanding of how to optimize GDL design is still being developed.

The GDL substrate is almost universally either a woven cloth or unwoven paper made from carbon fibers. Manufacturers often treat the GDL with hydrophobic fluoropolymer [4] and/or a granular microporous layer (MPL) or fill [5–7] in order to reduce the pooling of liquid water. The performance effects of different GDL treatment methods are normally evaluated using single-cell electrochemical measurements in the mass transfer affected regime [4–6,11,12]. Electrochemical measurements are governed by a complex set of coupled phenomena, making it difficult to reliably deconvolute the mass transfer affected response into a single factor such as the effect of GDL treatment on wetting properties. In situ visualization has helped to interpret such results, by illuminating some of the complex changes in liquid behavior that result from GDL modification [8–10]. Hydrophobic treatments have been shown to affect water movement throughout the entire cell, preventing spontaneous wicking of water into GDL pores [8,9], causing water to move as droplets instead of films in the gas channels [8,10], and even changing the water balance between anode and cathode sides of the cell [9,10]. However, a predictive understanding of such effects is still elusive, as the performance benefit of any GDL modification depends heavily on the specific operating conditions and cell geometry used. Moving forward, it will be important to connect treatment steps with quantitative measurements of the interaction of the GDL and liquid water. This paper seeks to provide such data, specifically addressing how the internal GDL pores change as a function

* Corresponding author. Tel.: +1 206 685 4815; fax: +1 206 685 3451.
E-mail address: dts@u.washington.edu (D.T. Schwartz).

0378-7753/$ – see front matter © 2009 Elsevier B.V. All rights reserved.
doi:10.1016/j.jpowsour.2009.08.032

Table 1
Select physical properties of the Toray TGP-H090 carbon fiber papers with increasing Teflon loadings.

Nominal Teflon loading[a]	Areal mass (mg cm^{-2})[b]	Calculated Teflon loading[c]	MIP cumulative volume (μL mg^{-1})[d]	Areal volume (μL cm^{-2})	Calculated porosity[e]
0 wt.%	11.9 ± 0.1	–	1.57	18.7 ± 1.0	0.67 ± 0.03
5 wt.%	12.7 ± 0.1	6.3 ± 1.1 wt.%	1.50	19.1 ± 1.0	0.68 ± 0.04
10 wt.%	13.1 ± 0.2	9.2 ± 1.4 wt.%	1.49	19.5 ± 1.1	0.70 ± 0.04
20 wt.%	14.8 ± 0.3	19.6 ± 1.6 wt.%	1.29	19.1 ± 1.2	0.68 ± 0.04
40 wt.%	21.5 ± 0.9	44.7 ± 2.4 wt.%	0.76	16.4 ± 1.9	0.59 ± 0.07

[a] Supplier-designated loading.
[b] Mean and uncertainty estimated from five measurements at each loading.
[c] Loading based on difference from 0 wt.% areal mass.
[d] Uncertainty estimated as ±0.08 μL mg^{-1} from three replicate measurements each of two carbon papers.
[e] Porosity based on the manufacturer-specified thickness of 280 μm.

of Teflon loading, a common parameter adjusted by manufacturers.

One very useful test that is rapidly gaining prominence for describing the GDL pore space is the capillary pressure-saturation measurement [13–20]. The capillary pressure, P_C, is the pressure difference formed between the liquid phase and gas phase within the pores of the GDL, expressed as a function of liquid saturation, S_L:

$$P_C(S_L) = P_L - P_G, \quad S_L = \frac{V_L}{V_{PORE}} = \frac{V_L}{\varepsilon V_T} \tag{1}$$

where P_L is liquid pressure, P_G is gas pressure, V_L is liquid volume, V_{PORE} is pore volume in the GDL, ε is material porosity, and V_T is total geometric volume of the GDL. The $P_C(S_L)$ curve provides a probe of the liquid/gas interfaces within the GDL material for different levels of water saturation. The simplest interpretation comes from the pressure in a smooth cylindrical capillary, expressed by the Young–Laplace equation [21]:

$$P_C = -\frac{2\gamma \cos\theta}{R_{EFF}} \tag{2}$$

where γ is the surface tension of an air/water interface, θ is the contact angle (as drawn through the liquid), and R_{EFF} is the effective pore radius. Although GDL materials do not have smooth cylindrical capillaries, Eq. (2) helps to understand the trends that can be observed through careful measurement of capillary pressure. Materials with smaller characteristic pores (smaller R_{EFF}) will increase the magnitude of capillary pressure required to intrude an interface past the pore throats, while hydrophobic treatments that lower surface energy (resulting in larger θ) shift the capillary pressure to more positive values. Moreover, this simple description belies a much more complex behavior, such as the hysteretic wetting/dewetting first shown in 2007 [14].

Here we show that the $P_C(S_L)$ relationship provides a sensitive fingerprint of the GDL material, and can be used as a direct probe for assessing how changes in manufacturing impact the morphology and wetting behavior of the material. There are several ways to extract parameters that are useful for interpreting changes in GDL properties. Harkness et al. suggested comparing two quantities from $P_C(S_L)$ measurements with fuel cell water management performance, namely, the "modal imbibition pressure" and the pressure/saturation required to sustain a 1.5 A cm^{-2} equivalent liquid flow [19]. Gostick et al. suggested using $P_C(S_L)$ data to calculate the USBM wettability index, a ratio of the work required to dewet vs. wet a GDL sample [20]. We recently showed that a bundle-of-capillaries model can be used for a self-consistent interpretation of apparent GDL pore size distribution and hysteretic contact angle distribution from mercury intrusion porosimetry (MIP) and $P_C(S_L)$ experiments [22]. Despite oversimplifying both the structure and wetting physics of complex porous media, bundle-of-capillaries models are commonly used for understanding MIP experiments [23], and we show that they are valuable for comparing the interaction of GDL materials and water.

2. Experimental

In this study, a series of Toray carbon papers was tested with increasing Teflon loadings to quantify the impact of the coatings on liquid water interaction. All GDL samples tested were Toray TGP-H090 carbon papers either left plain or commercially wetproofed by the supplier. Papers were tested with nominal loadings of 5 wt.% Teflon (Fuel Cell Earth, Stoneham, MA) as well as 10, 20, and 40 wt.% Teflon (BASF Fuel Cell, Somerset, NJ). Although the details of wetproofing treatment are proprietary to the suppliers, it is commonly accomplished through deposition of a suspension of polytetrafluoroethylene (PTFE) or fluorinated ethylene propylene (FEP) particles [4,24,25], and will be treated as such in our discussion. Measured physical properties are summarized in Table 1; sample thickness was taken as the manufacturer-specified 280 μm.

2.1. Mercury porosimetry

A Micromeritics AutoPore IV 9500 was used for mercury intrusion porosimetry (MIP) experiments. Mercury pressure was increased from 0.4 to 30,000 psi (3 kPa–207 MPa), and the corresponding intruded volume was measured; a maximum volume was reached for each carbon paper sample well below the final pressure. The cumulative volume intruded was taken as the total pore volume. Incremental volume intruded at each pressure was used to estimate a pore size distribution for each sample according to Eq. (2). The mercury/vapor surface tension was taken as 0.485 N m^{-1}, and the assumed contact angle was 130°.

2.2. Water/air capillary pressure

A schematic of the setup used to measure water $P_C(S_L)$ relationships is shown in Fig. 1. The equipment used was similar to a pressure cell described previously [22], but the incorporation of the GDL sample into the cell was improved. The epoxy previously used to seal the edges of the sample was eliminated out of concern for potential changes in the wettability and pore volume of the material. Instead, the following scheme was used to seal the sample within the cell: the 38 mm diameter GDL sample (a) was encircled by a 20 mil Teflon gasket (b) and sandwiched between a hydrophobic Teflon membrane (c, Pall Life Sciences TF-450, 0.45 μm characteristic pores) and a hydrophilic Nylon membrane (d, Whatman NL 17, 0.45 μm). Both membranes were supported by a 4 mil thick stainless steel screen (e, Pall Corporation) perforated with 180 μm pores. This sample stack was assembled between the two halves of an aluminum pressure cell, with distributor flow fields machined into the two mating faces. The sample stack was sealed by two o-rings that crush the membranes and

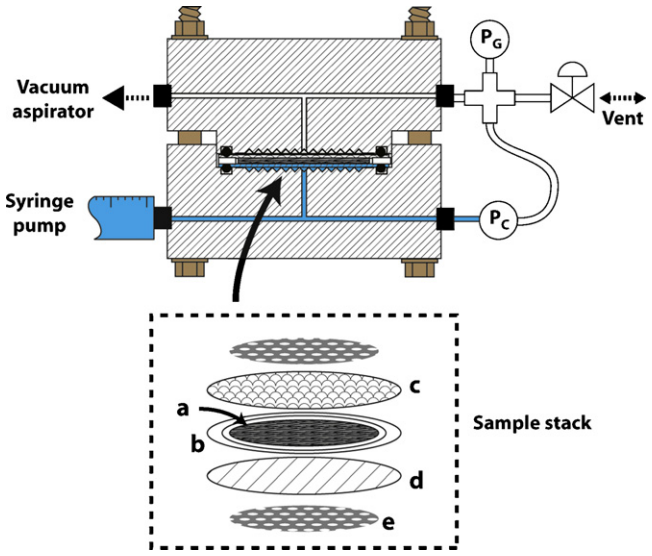

Fig. 1. Schematic for the capillary pressure measurement apparatus. The GDL sample (a) is surrounded by a Teflon gasket (b) and sandwiched between hydrophobic (c) and hydrophilic (d) membranes. Each membrane is supported by a steel screen (e). This sample stack is compressed between the two manifolds of the pressure cell. After assembly, the cell is evacuated using a vacuum aspirator, the vent valve is used to set the gas pressure measured by transducer P_G. The bottom manifold and sample stack are filled with liquid water using the syringe pump, then the vacuum aspirator is turned off. The saturation is then cycled using the syringe pump and the capillary pressure difference is measured by transducer P_C.

Teflon gasket around the perimeter of the GDL sample. The torque on the assembly bolts was set with a torque wrench and the resulting compressive pressure on the GDL sample was estimated using pressure-sensitive film (Sensor Products Inc.). For all data presented here, the pressure on the samples was estimated to be approximately 85 psi (0.59 MPa). This was found to be sufficient to compress the membranes tightly against the GDL sample and maintain fluid contact across the layers, and represented a moderate compressive force compared to what is used in some fuel cell stacks [26].

The procedure for measuring capillary pressure was nearly identical to that described previously [14,22]. Briefly, after the liquid manifold and sample were filled under vacuum [22], the syringe pump was used to cycle water at a constant rate into and out of the sample while the liquid/gas pressure difference was measured. After verifying that the water intrusion and gas intrusion curves were consistent, a stepwise cycle was taken; the final capillary pressure was recorded after a pause of 120 s after each volume change step [14]. The saturation at each step was calculated as in Eq. (1), with the sample assumed to be completely drained at −30 kPa (i.e. zero irreducible saturation assumed) and the liquid volume at pressures above −30 kPa indicated by the change in the syringe volume. The total pore volume was taken from MIP total intrusion volume. The air manifold was left stagnant during the test, as this was found to prevent evaporation more effectively than humidifying the gas side by sparging.

2.3. Imaging methods

The coating quality was observed using two imaging techniques, scanning electron microscopy (SEM) measuring backscattered electron intensity and time-of-flight secondary ion mass spectroscopy (ToF-SIMS). SEM backscattering (SEM-B) has previously been used to look at GDL coatings, as fluoropolymer additives appear white due to the higher rate of elastic interactions compared to graphitic carbon [24]. Here we use a JEOL JSM-7000F at 10 keV accelerating voltage operating in backscattered electron mode. The technique has limited surface sensitivity, so it is mainly useful for identifying areas thickly coated in Teflon. ToF-SIMS is complementary to SEM-B, as it probes the top few nanometers of a sample and thus reveals Teflon thin films down to the sub-monolayer level. Areas of 0 and 5 wt.% samples were windowed with carbon tape so that the same area could be compared with both imaging methods. ToF-SIMS spectra were acquired on an ION-TOF TOF.SIMS 5 spectrometer using an 25 keV Bi_3^+ ion source in pulsed mode, for a mass range of $m/z = 0$–500.

2.4. Fitting effective contact angle distribution with bundle-of-capillaries model

Water/air $P_C(S_L)$ curves for each carbon paper were fit using a bundle-of-capillaries model as described previously [22]. Briefly: a pore size distribution for each nominal Teflon loading was first estimated using the MIP incremental volume. A series of normalized single-Gaussian contact angle distributions was then assumed, each with a given mean contact angle θ_{mean} and standard deviation σ. No correlation was assumed between contact angle and pore radius, so smaller pores had the same contact angle distribution as larger pores. A MATLAB script was used to calculate theoretical water/air $P_C(S_L)$ curves for a bundle of cylindrical capillaries using Eq. (2) for each contact angle distribution, and the best fit for the corresponding experimental $P_C(S_L)$ curve was found from the lowest root sum of squared error (RSSE), using a weighting scheme that reduced the influence of the less certain low and high pressure extremes. For the experimental $P_C(S_L)$ curves that were fitted, an effective saturation was used that removed the irreducible and residual phase saturations, as a bundle-of-capillaries model cannot include trapped phases. Effective liquid saturation, $S_{E,L}$, was calculated as follows [22]:

$$S_{E,L} = \frac{S_L - S_{L,Min}}{S_{L,Max} - S_{L,Min}} \quad (3)$$

where $S_{L,Min}$ is irreducible liquid saturation (corresponding to the volume at roughly −20 kPa capillary pressure for these Toray samples) and $S_{L,Max}$ is the maximum liquid saturation (residual gas saturation, corresponding to +20 kPa). The surface tension of the water/air interface was taken as 0.072 N m^{-1}.

3. Results and discussion

3.1. Mercury porosimetry

Cumulative pore volume plots from mercury intrusion porosimetry are shown in Fig. 2a. There is no systematic trend in total areal volume among papers with 0–20 wt.% Teflon loading, and we conclude that lot-to-lot variability in the porosity of the carbon substrate is comparable to the volume lost to the Teflon treatment. A significant drop in areal pore volume is observed with the 40 wt.% paper, which was confirmed by gravimetric measurement of samples spontaneously wetted with isopropanol. Fig. 2b shows that there is a slight shift in the characteristic pore radius (where the majority of volume is intruded) from approximately 14–13 μm from papers with 0–40 wt.%, respectively. This is consistent with deposits of fluoropolymer particles reducing the effective pore throat sizes between the carbon fibers, but the effect is not large. For a smooth cylindrical pore, this shift in characteristic pore size would result in a pressure increase of about 8%, which is comparable to our sample-to-sample variability.

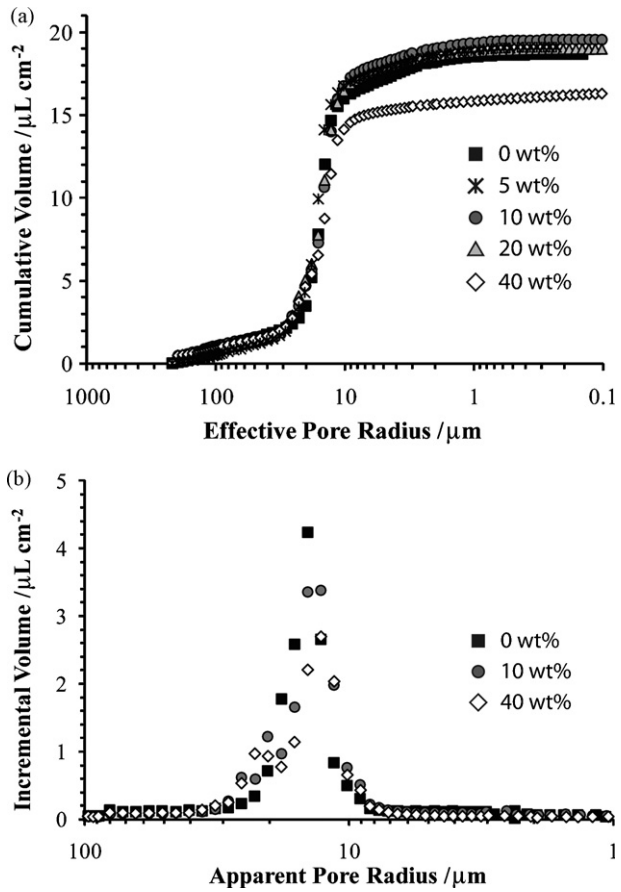

Fig. 2. Mercury intrusion porosimetry data for Toray TGP-H090 wetproofed with 0 wt.% (squares), 5 wt.% (stars), 10 wt.% (circles), 20 wt.% (triangles), and 40 wt.% Teflon (diamonds): (a) cumulative intruded volume as a function of apparent pore radius. The total pore volume only shows a significant drop with the addition of 40 wt.% Teflon. (b) Incremental pore volume.

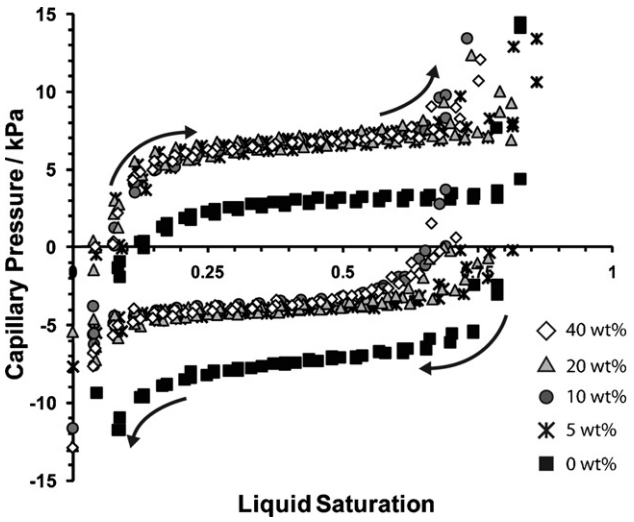

Fig. 3. Liquid intrusion and gas intrusion water/air capillary pressure curves for Toray TGP-H090 carbon papers, three replicate samples for each condition: plain carbon paper (squares), and wetproofed with 5 wt.% (stars), 10 wt.% (circles), 20 wt.% (triangles), and 40 wt.% Teflon (diamonds). A significant shift to more positive (more hydrophobic) capillary pressures was observed between plain and 5 wt.% Teflon loaded paper. Higher loadings did not further shift the magnitude of the capillary pressure for most of the saturation range.

3.2. Water/air capillary pressure

Capillary pressure curves for Toray papers with 0, 5, 10, 20 and 40 wt.% Teflon loading are shown in Fig. 3. Data for three replicate samples at each loading are included. One noticeable feature is the large hysteresis observed between liquid intrusion and gas intrusion curves. Liquid intrusion required positive liquid pressures to increase saturation, while gas intrusion required negative liquid pressures to decrease saturation. There was almost zero spontaneous imbibition or drainage (liquid intrusion at negative pressures or gas intrusion at positive pressures), meaning liquid saturation will remain static in these materials until applied external pressure exceeds the pressure required to force fluid fronts through additional pore throats. This hysteresis has been observed by multiple researchers measuring capillary pressure curves in carbon papers, all recording characteristic pressures in the range of 2–10 kPa [14,18,19]. It has been noted that structural effects from the complex pore geometry of the fibrous materials is sufficient to explain the hysteresis [18,19], though chemical heterogeneity may also play a role [22].

Comparing curves for 0 and 5 wt.% loaded samples, pressures for the entire saturation range are seen to shift to more positive values with this first addition of Teflon. This reflects the expected lowering of surface energy as graphitic carbon is covered by the fluoropolymer. This effect is observed for both liquid intrusion and gas intrusion processes, but the large hysteresis between the two curves is maintained. That is, a higher positive pressure is required to force water into the GDL pores (around 4 kPa increase between 0 and 5 wt.% Teflon), but a less negative pressure is required to remove liquid from the same pores. Comparing the magnitude of liquid intrusion and gas intrusion curves, for the 0 wt.% (bare carbon) samples it is easier to intrude water than it is to remove it, while for the wetproofed samples it is easier to remove water than to intrude it. Gostick et al. suggested using the USBM wettability index to quantify this effect of Teflon loading [20], where a negative value will clearly show that it was easier to dewet a sample than it was to wet it. Our calculated wettability indices are +0.47 and −0.26 for the plain and 5 wt.% treated papers, respectively, comparing favorably with Gostick et al.'s values for similar materials.

Above 5 wt.%, additional Teflon loading has negligible effect on capillary pressure for both the liquid intrusion and gas intrusion processes. The pressures required for the liquid or gas front to penetrate pore throats does not rise systematically with higher loadings, as might be expected. Additional fluoropolymer is apparently not covering bare carbon, but is instead thickening the existing coat of Teflon, as was suggested previously by Gostick et al. [20]. Further evidence for this conclusion is discussed in Section 3.3. The minor geometry changes from thicker Teflon deposits (as discussed in Section 3.1) are also apparently too small to affect the movement of water/air interfaces, with the possible exception of the gas intrusion pressures at high saturation.

Some previous studies have suggested that increasing Teflon loading has little effect decreasing water wettability above some minimum threshold value. Using meniscus height measurements, Lim and Wang found that external contact angles on treated carbon papers were not significantly different between 10 and 40 wt.% Teflon [4]. Using octane drainage and the method of standard porosimetry, Kumbur et al. found a small difference between 10 and 20 wt.% loaded SGL papers, but the difference was much less than that observed between 5 and 10 wt.% papers [15]. In measuring a "hydrophobia fraction", Lobato et al. recorded significant spontaneous uptake of liquid water for an untreated Toray substrate, but almost none for E-Tek paper from 40 wt.% down to 10 wt.% Teflon [11]. Finally, Gostick et al. found no significant difference in capillary pressure between E-Tek carbon papers loaded with 10 and 20 wt.% Teflon [20].

Other studies have shown significant differences between GDLs measured at higher Teflon loadings, suggesting that the coating was not complete in these cases. Vol'fkovich et al. observed significantly more spontaneous uptake of liquid water for Teflon loadings less than their maximum of 42 wt.% [25]. Cheng et al. observed decreases in the reactivity of the carbon surface with oxygen past loadings of 20 wt.% [24].

It is difficult to draw broad conclusions from these results; some suggest that additional Teflon above 10 wt.% has very little impact on coating while others observe large changes for loadings beyond 40 wt.%. The different techniques do look at different aspects of the GDL; i.e. external contact angle is only affected by surface wettability while reactivity with oxygen is determined by the carbon surface throughout the GDL, and even capillary pressure is determined by restricting pore throats and may be unaffected by changes in the larger pore spaces. Differences may also arise from the individual coating techniques and the specific fluoropolymer used for each study. Additional study is required using these complementary techniques in order to determine optimum loading level for a given treatment method and material.

3.3. Imaging of Teflon coverage

SEM backscattering micrographs of the 0, 5, and 10 wt.% wetproofed carbon paper surfaces are shown in Fig. 4. Image contrast is based in part on the rate of elastic electron scattering, making thick deposits of fluoropolymer appear white against the background of carbon fibers and binder material. Arrowheads highlight several thick Teflon regions in Fig. 4b and c. With a 5 wt.% Teflon loading (Fig. 4b), the fluoropolymer mainly appears as deposits limited to corners and the junctions between fibers, and large areas of carbon appear exposed. Similar heterogeneous distributions of Teflon have been commonly observed for GDL carbon papers [4,24,27]. The heterogeneous distribution has been explained by the fluoropolymer application process and redistribution during the subsequent drying and sintering steps. For the 10 wt.% sample (Fig. 4c), the white contrast appears to show that the Teflon is much more widespread with the slightly heavier loading, and much less exposed binder is visible. Bridges and films of Teflon are also visible at pore corners; such films have been noted as a major effect of higher Teflon loadings due to their impact on transport [4].

Insets in Fig. 4a and b show ToF-SIMS maps of the CF_2^+ ion signal ($m/z = 50$) for the 0 and 5 wt.% Teflon samples. The corresponding areas on the SEM micrographs are indicated by dashed boxes. Comparable images were generated for all significant positive and negative ion PTFE peaks and gave similar indications of Teflon surface coverage. The CF_2^+ signal (bright pixels) for the untreated paper (Fig. 4a inset) corresponds to noise levels, confirmed by examining the full ToF-SIMS spectrum. In contrast, the full spectrum and ion map images for the 5 wt.% wetproofed material shows that fluoropolymer is ubiquitous in the sample. Comparing the SEM and ToF-SIMS images in Fig. 4b shows that Teflon functionality is present where there are no deposits visible in the SEM. The only dark areas in the inset appear where there is shadowing of the ion beam by topography.

Fluoropolymer functionality is observable everywhere on the surface at the lowest Teflon loading tested, which helps to explain the insensitivity of $P_C(S_L)$ measurements at higher Teflon loadings. Based on the apparent Teflon coverage from SEM backscattering, it might be expected that the 5 and 10 wt.% samples would show a significant difference in wetting behavior. However, the more surface-sensitive ToF-SIMS technique suggests that the fluoropolymer is present far beyond the thick deposits that show contrast in the SEM. The ubiquitous thin coating is important, since wetting is generally dominated by the top few monolayers of a surface [28]. Higher loadings of Teflon on the GDL materials will only add to this base coating and are unlikely to change the wetting or the capillary pressure, which supports a previous suggestion by Gostick et al. [20].

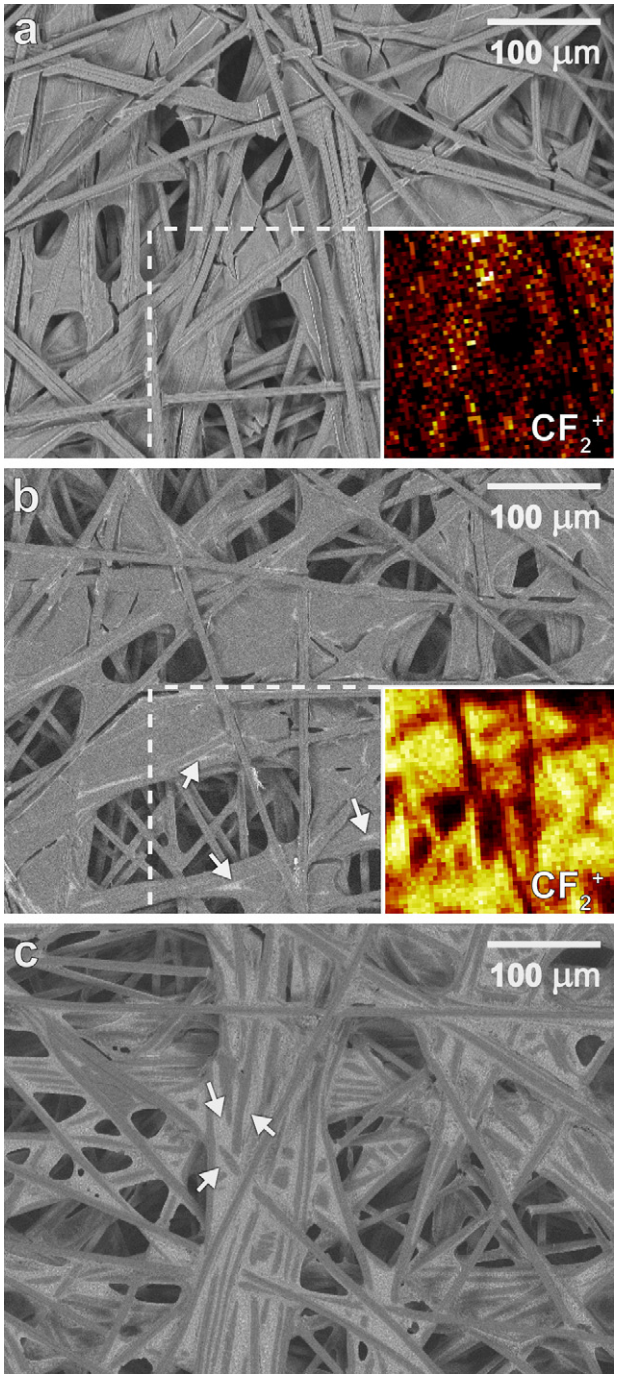

Fig. 4. SEM backscattering micrographs of Toray TGP-H090 samples with nominal Teflon loadings of (a) 0 wt.% (b) 5 wt.% and (c) 10 wt.%. Arrows highlight several thick fluoropolymer deposits. Insets show ToF-SIMS images for CF_2^+ peak ($m/z = 50$) for the boxed areas on the 0 and 5 wt.% samples; brighter pixels correspond to stronger signal.

This more widespread thin coating is likely a result of the typical wetproofing treatment process used for GDL materials. The final sintering step takes the sample temperature far above the glass transition temperature of the deposited Teflon particles, and often above the melting point. At these temperatures, the polymer has high mobility and may spread across the graphitic substrate. This effect will be more important when a Teflon copolymer such as

Table 2
Best fit parameters for a single-Gaussian contact angle distribution.

Nominal Teflon loading	Intruding phase	Mean contact angle θ_{mean} (°)	Standard deviation θ (°)
0 wt.%	Liquid	104.0	4.0
	Gas	31.6	11.6
5 wt.%	Liquid	132.7	1.7
	Gas	66.7	1.0
10 wt.%	Liquid	130.8	1.0
	Gas	69.6	1.0
20 wt.%	Liquid	130.7	1.0
	Gas	66.3	1.0
40 wt.%	Liquid	130.7	1.0
	Gas	68.8	4.0

FEP is used as the treating agent, as the lower molecular weight copolymers are more mobile at high temperature than pure PTFE [29]. Hence, the final quality and uniformity of the wetproofing treatment can be adjusted by changing the Teflon copolymer or by altering the conditions of the high-temperature treatment steps. In the case of the commercially treated carbon papers considered in this study, the surface chemistry as revealed by ToF-SIMS shows that the treatment has already been optimized to provide high Teflon coverage.

3.4. Fitting effective contact angle distribution with bundle-of-capillaries model

Using the pore size distribution calculated from MIP, effective contact angle distributions for each sample were estimated, assuming a bundle-of-capillaries model and a single-Gaussian distribution, using the method detailed in Cheung et al. [22]. Parameters resulting in the best fit for each experimental P_C–S curve are listed in Table 2, and the experimental capillary pressure data and fitted curves for Toray TGP-H090 with Teflon loadings of 0, 5 and 10 wt.% are shown in Fig. 5a. The effective contact angle distributions for these loadings are plotted in Fig. 5b.

The effective mean contact angles for both water intrusion and gas intrusion rise as Teflon loading increased from 0 to 5 wt.%, but do not continue to increase at higher loadings. This again indicates that the fluoropolymer coating lowers the surface energy with the minimal addition of Teflon but has no additional effect at higher loadings for these papers. The mean contact angles for liquid intrusion into the wetproofed samples are in the range of 130–133°. This is the middle of the range estimated by Harkness et al., who compared "modal imbibition pressures" for mercury and water for three wetproofed GDLs [19].

The calculated distributions become much narrower with increasing Teflon loading, as reflected in the shrinking standard deviations. A standard deviation of one degree was the smallest value included in our investigated range, so the distributions approach δ-functions for most Teflon loadings. Careful examination shows that this is because the fitted $P_C(S)$ curves with the lowest RSSE are not quite able to match the experimental data for the Teflon-treated samples. The fitted curves are too negative at low saturations and too positive at high saturations. This effect comes from the shape of the MIP pressure curves used to calculate pore size distributions, reflecting differences in the way the samples were encased in the MIP apparatus vs. in the water/air capillary pressure cell (i.e. uncompressed vs. moderately compressed).

It is worth noting that the calculated mean contact angles for water intrusion into the wetproofed papers are very close to our assumed contact angle for mercury intrusion (130°, used to calculate pore size distribution). It appears that, when the effect of surface tension is removed, it is just as difficult for water to penetrate this material as it is for mercury. From the combination of pore roughness and lowering of surface energy from Teflon, the water/air interface behavior approaches the highly non-wetting behavior of the mercury/mercury vapor interface, even for a 5 wt.% Teflon loading. Based on this observation, if a larger resistance to water intrusion is desired for better water management, it will probably have to come from a change in pore geometry and not in wetting.

Another conclusion is that MIP can sometimes be used to approximate the water intrusion curve for an effectively Teflonated material, with a simple ratio of surface tensions, γ_{H2O}/γ_{Hg}, required

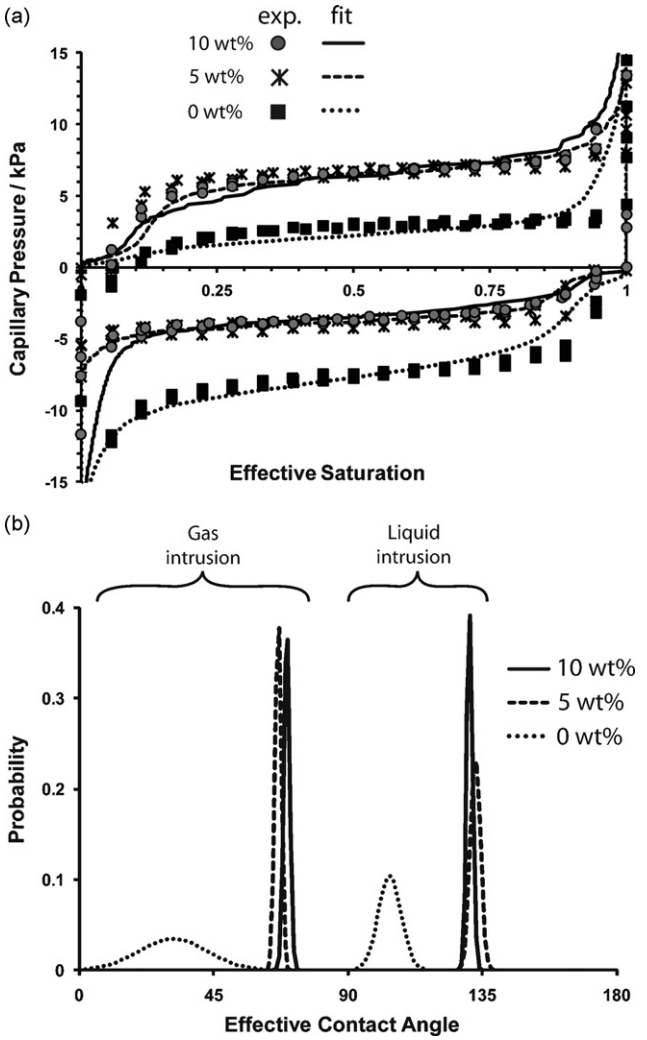

Fig. 5. Fitting of capillary pressure data using a bundle-of-capillaries model with pore size distribution from mercury intrusion. (a) Capillary pressure data and fits for Toray TGP-H090, plain (squares and dotted line) and treated with 5 wt.% (stars and dashed line) and 10 wt.% Teflon (circles and solid line). Effective saturation for each curve was calculated using Eq. (3). (b) Calculated contact angle distributions for the fitted curves.

for conversion. This validates an assumption previously used by Acosta et al. to estimate water intrusion pressures from mercury intrusion of carbon cloth [30]. In that case, the cosine of the each contact angle was also included in the conversion, but the measured contact angles for mercury and water on the rough surface of the carbon cloth were nearly identical (141° vs. 143°). It has similarly been observed that for highly wetting or non-wetting fluids in a rough pore space, it is often more accurate to ignore contact angle for such conversions [31].

MIP alone cannot be used to estimate water intrusion pressures for GDLs with significant bare carbon exposed. In such cases, the wetting difference between mercury and water is more significant than the effects of pore roughness. Some estimate of the effective contact angle difference would be required, such as those calculated in this study.

We acknowledge that the GDL material does not physically resemble a bundle-of-capillaries, and the complex geometry and connectivity of the fibrous pore space play major roles in the observed hysteresis between liquid and gas intrusion. Therefore, the different contact angle distributions calculated here should be viewed as effective contact angles and not a direct result of the wettability of the surfaces. However, this phenomenological approach is useful for describing changes in wetting (as revealed by water/air capillary pressure) and separating out the impact of geometry changes (as shown by MIP). Furthermore, the use of effective advancing and receding contact angles is one way of accounting for hysteretic effects in pore network models without including complex geometric effects (pinned interfaces, etc), and therefore assigning effective contact angle distributions can be helpful in modeling GDL behavior. For example, contact angle hysteresis has been used to model hysteretic capillary pressure relationships in "corrugated" pore networks, essentially pore networks with a connectivity of two [32].

4. Conclusions

Commercial carbon paper GDLs with increasing Teflon loading were investigated to quantify the impact of fluoropolymer coating on the interaction with liquid water. Mercury porosimetry showed a very small decrease in the characteristic pore size for Teflon loadings up to 40 wt.%. Hysteretic water/air $P_C(S_L)$ curves shifted to more positive pressures with the addition of 5 wt.% Teflon, but no further change was found between 5 and 40 wt.% loading. ToF-SIMS imaging confirmed that the fluoropolymer coverage was nearly complete at 5 wt.% loading, indicating that the wetproofing agent was able to spread during high temperature treatment.

A bundle-of-capillaries model was used to calculate effective pore size distributions for water and gas intrusion into each sample. The effective mean contact angles rose with the initial addition of Teflon, reflecting the lowering of GDL surface energy, but with no further increase above 5 wt.% loading. The calculated contact angle distribution for water intrusion approached a delta function around the assumed contact angle for mercury, indicating that the water intrusion process was comparable to mercury intrusion for these treated carbon papers.

The samples tested in this study were effectively wetproofed, with a rough Teflonated pore space that required only very low fluoropolymer loadings to be effective. We conclude that: (1) because of insensitivity to the specific loading used, water wetting should be a lesser consideration compared to the other effects of increased Teflon treatment, such as changes to permeability, tortuosity and mechanical strength [4,11]; and (2) future efforts to optimize the GDLs for high current density operation should focus on engineering pore geometry, as the surface coating is less likely to provide further gains.

It is worth noting that these conclusions were based on tests with new GDL samples at room temperature, reflecting the properties of the materials when a fuel cell is first assembled. There is much work showing that the GDLs lose hydrophobicity during the course of a PEMFC lifetime [2]. Also, GDL wettability has been observed to shift to more hydrophilic behavior after exposure to liquid water at fuel cell operating temperatures [4,25]. Water/air capillary pressure measurements like those described here will be very useful in quantifying these changes for different GDL materials, and in improving designs to compensate for these effects, and these changes will be explored in a future study.

Acknowledgements

The authors would like to thank Tuesday Kuykendall of UW MSE for acquiring the MIP data and Jim Hull at NESAC/BIO (supported by NIH grant #EB-002027) for the ToF-SIMS images. This work was partially supported by a Ford Motor Company Fellowship (to Joseph D. Fairweather), the Boeing-Sutter Endowment for Excellence in Engineering, and NSF grant #0654252.

References

[1] H. Li, Y.H. Tang, et al., J. Power Sources 178 (2008) 103–117.
[2] R. Borup, J. Meyers, et al., Chem. Rev. 107 (2007) 3904–3951.
[3] W. Schmittinger, A. Vahidi, J. Power Sources 180 (2008) 1–14.
[4] C. Lim, C.Y. Wang, Electrochim. Acta 49 (2004) 4149–4156.
[5] J.M. Song, S.Y. Cha, et al., J. Power Sources 94 (2001) 78–84.
[6] F. Lufrano, E. Passalacqua, et al., J. Appl. Electrochem. 29 (1999) 445–448.
[7] J.T. Gostick, M.A. Ioannidis, et al., Electrochem. Commun. 11 (2009) 576–579.
[8] K. Tuber, D. Pocza, et al., J. Power Sources 124 (2003) 403–414.
[9] S. Ge, C.Y. Wang, J. Electrochem. Soc. 154 (2007) B998–B1005.
[10] D. Spernjak, A.K. Prasad, et al., J. Power Sources 170 (2007) 334–344.
[11] J. Lobato, P. Canizares, et al., J. Appl. Electrochem. 38 (2008) 793–802.
[12] V.A. Paganin, E.A. Ticianelli, et al., J. Appl. Electrochem. 26 (1996) 297–304.
[13] J.T. Gostick, M.W. Fowler, et al., J. Power Sources 156 (2006) 375–387.
[14] J.D. Fairweather, P. Cheung, et al., Electrochem. Commun. 9 (2007) 2340–2345.
[15] E.C. Kumbur, K.V. Sharp, et al., J. Electrochem. Soc. 154 (2007) B1295–B1304.
[16] T.V. Nguyen, G. Lin, et al., Electrochem. Solid-State Lett. 11 (2008) B127–B131.
[17] K.G. Gallagher, R.M. Darling, et al., J. Electrochem. Soc. 155 (2008) B1225–B1231.
[18] J.T. Gostick, M.A. Ioannidis, et al., Electrochem. Commun. 10 (2008) 1520–1523.
[19] I.R. Harkness, N. Hussain, et al., J. Power Sources 193 (2009) 122–129.
[20] J.T. Gostick, M.A. Ioannidis, et al., J. Power Sources 194 (2009) 433–444.
[21] J. Bear, Dynamics of Fluids in Porous Media, American Elsevier Pub. Co, New York, 1972.
[22] P. Cheung, J.D. Fairweather, et al., J. Power Sources 187 (2009) 487–492.
[23] F.A.L. Dullien, Porous Media: Fluid Transport and Pore Structure, Academic Press, New York, 1979.
[24] D. Cheng, S.Y. Ye, et al., Electrochem. Solid-State Lett. 11 (2008) B148–B152.
[25] Y.M. Vol'fkovich, V.E. Sosenkin, et al., Russ. J. Electrochem. 44 (2008) 278–285.
[26] W.K. Lee, C.H. Ho, et al., J. Power Sources 84 (1999) 45–51.
[27] D. Bevers, R. Rogers, et al., J. Power Sources 63 (1996) 193–201.
[28] G.M. Whitesides, P.E. Laibinis, Langmuir 6 (2002) 87–96.
[29] C.W. Stewart, R.C. Sheland, et al., J. Vinyl Addit. Technol. 4 (1998) 229–232.
[30] M. Acosta, C. Merten, et al., J. Power Sources 159 (2006) 1123–1141.
[31] W.G. Anderson, J. Petrol. Technol. 39 (1987) 1283–1300.
[32] C. Salmas, G. Androutsopoulos, J. Colloid Interface Sci. 239 (2001) 178–189.